International Journal of Hydrogen Energy 270 (2026) 157013

Contents lists available at ScienceDirect

International Journal of Hydrogen Energy

journal homepage: www.elsevier.com/locate/he

Review Article

Power electronic converters for green hydrogen production from photovoltaic: A review

Paolo Pilati [a], Riccardo Mandrioli [a], Vincenzo Cirimele [a], Mattia Ricco [a],*, Damien Guilbert [b]

[a] Department of Electrical, Electronic and Information Engineering, University of Bologna, Viale del Risorgimento 2, Bologna, 40126, Italy
[b] GREAH, Université Le Havre Normandie, 75 rue Bellot, 76600, Le Havre, France

ARTICLE INFO

Keywords:
Electrolyzer
Green hydrogen
Photovoltaic
Power electronics

ABSTRACT

The increasing penetration of renewable energy sources has intensified the need for efficient energy storage solutions to mitigate their intermittent nature. Among available options, hydrogen is a promising energy carrier, with water electrolysis representing the most established pathway for sustainable production. Conventionally, photovoltaic (PV) energy is processed through the AC grid before supplying electrolyzers, although both systems inherently operate in DC. Direct PV-to-electrolyzer coupling can therefore improve efficiency by reducing conversion stages and associated losses. This paper reviews the state of the art in power electronic converters for direct coupling of PV sources and electrolyzers. The electrical characteristics of both systems are first analysed to identify converter requirements. Subsequently, isolated and non-isolated converter topologies are compared in terms of voltage conversion capability, electrolyzer current ripple, and component count. Finally, emerging research directions are discussed, including modular converter architectures and the opportunities enabled by advanced semiconductor technologies.

Contents

* Corresponding author.
E-mail addresses: paolo.pilati3@unibo.it (P. Pilati), r.mandrioli@unibo.it (R. Mandrioli), vincenzo.cirimele@unibo.it (V. Cirimele), mattia.ricco@unibo.it (M. Ricco), damien.guilbert@univ-lehavre.fr (D. Guilbert).
URLs: https://www.unibo.it/sitoweb/r.mandrioli (R. Mandrioli), https://www.unibo.it/sitoweb/vincenzo.cirimele (V. Cirimele), https://www.unibo.it/sitoweb/mattia.ricco (M. Ricco).

https://doi.org/10.1016/j.ijhydene.2026.157013
Received 12 February 2026; Received in revised form 16 June 2026; Accepted 10 August 2026
Available online 25 August 2026

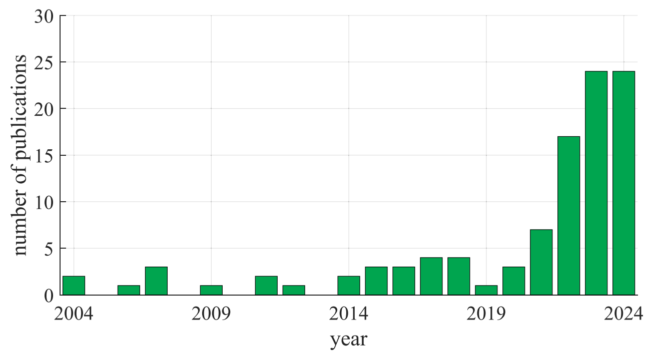

Fig. 1. Number of publications per year about converters for PV–Electrolyzer applications.

1. Introduction

The problem of climate-altering gas emissions and the consequent climate change [1] have led to a significant increase in the production of energy from renewable sources in recent years, particularly photovoltaic (PV) and wind power [2]. However, a primary characteristic of these sources is that they are not programmable, but rather depend heavily on ambient conditions. It is therefore necessary to find systems for storing energy, so that it can be accumulated when produced in excess and then used when needed [3]. There are already various storage solutions on the market, from water pumping to batteries, but one form that has gained particular interest in recent years is hydrogen.

Hydrogen is not a primary energy resource, as it is not found freely in nature; however, due to its properties, it can be used as an energy carrier or to decarbonize hard-to-abate industries [4,5]. It is currently mainly used as a raw material in industrial processes, being produced from hydrocarbons [6]. Hydrogen can be produced renewably in various ways [7,8], but the most established technique is the electrolysis of water [9]. In recent years, therefore, hydrogen production by electrolysis has attracted the interest of both policymakers and the scientific community. Since 2020, the European Union has funded numerous projects for the construction of plants for the production of hydrogen from renewable sources. Plants sizes range from MW, up to GW [10]. In many cases, the renewable source used is PV, especially for all those projects based in southern European countries, where there is a greater availability of sunshine hours [11]. About the scientific interest in finding optimal solutions for the development of this technology, Fig. 1 shows the trend over the past twenty years in the number of publications relating solely to power electronic converters for the production of hydrogen from PV. The graph was created by consulting generic search engines such as Google Scholar and more specific databases, such as ScienceDirect and IEEExplore, using the following as keywords for searching: "power converters photovoltaic electrolyzer". As can be seen, the trend has increased significantly in recent years.

The current state of the art for hydrogen production from PV involves the use of separate converters for the PV part and the electrolyzer. In particular, to maximize the production of the electrolyzer, a grid connection is always considered. Thus, most plants currently employ rectifiers of various types to feed the electrolyzers, while the PV is connected to the grid via inverters [12–15]. But, since both PV and electrolyzers are, respectively, DC sources and loads, the intermediate step of converting to AC is superfluous and may cause a reduction in overall system efficiency. It is also possible to directly connect PV and electrolyzer [16–20], but no control over the system would be achieved. This could lead to both components being operated in a sub-optimal working point [21,22]. Even if the presence of the grid is considered to provide balancing services, conversion to AC would not be strictly necessary [23–25]. In Fig. 2, an outline comparison of the current state-of-the-art plant layout for hydrogen production from renewable sources and what could be a possible future configuration is given.

As this is therefore a sector with considerable potential for development, numerous converter topologies, coupling configurations between PV and electrolyzers, and control algorithms have been studied in recent years. There are already reviews in the literature dealing with the state of the art for electrolyzer converters, whether considering an AC source [26–30] or a generic DC source [26,29,31,32]. In all the cases just mentioned, however, the main focus is on the load (the electrolyzer), while the source is considered ideal. The only review that really considers coupling with PV is [33], which, however, only focuses on converter efficiency. In this paper, the current status of the converters' development for the hydrogen production from PV is reported, with particular reference to the most popular topologies, their conversion ratio, current ripple, and control techniques.

The article is organized as follows: in Section 2 an overview of the PV and electrolyzer component is reported, highlighting the converter's requirement, in Section 3 the current situation on non-isolated topologies is discussed, while Section 4 deals with isolated topologies, Section 5 provides a summary discussion and Section 6 a discussion of possible future developments of this application.

2. Basics on PV-electrolyzer system

This Section deals with the main components of the system in question: the electrolyzer and the photovoltaic generator. In particular, their electrical characteristics will be described to point out which features are sought in the converters associated with them.

2.1. Electrolyzer characteristics

In water electrolysis, electrical energy is used to split water into hydrogen and oxygen. Under reversible conditions (open-circuit), the required cell voltage E is given by [34]:

$$E = -\frac{\Delta G}{2F} , \tag{1}$$

where ΔG is the Gibbs free energy variation and F is the Faraday constant. Since Eq. (1) only applies under ideal reversible conditions, real electrolytic cells must also account for activation, ohmic, and diffusion losses [34]. Activation losses dominate at low current densities, ohmic losses in the normal operating region, while diffusion losses occur beyond the rated current density and are generally avoided because they accelerate electrolyzer degradation.

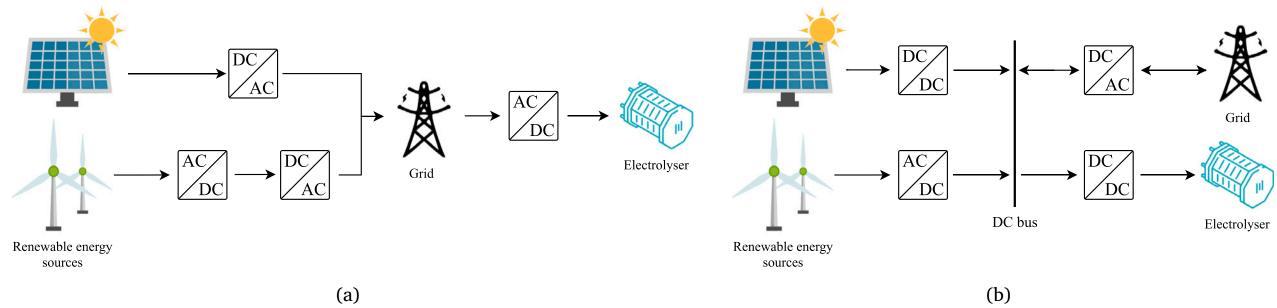

Fig. 2. Possible configurations for hydrogen production plant from renewable energy sources: (a) current state-of-the-art, and (b) future possibilities.

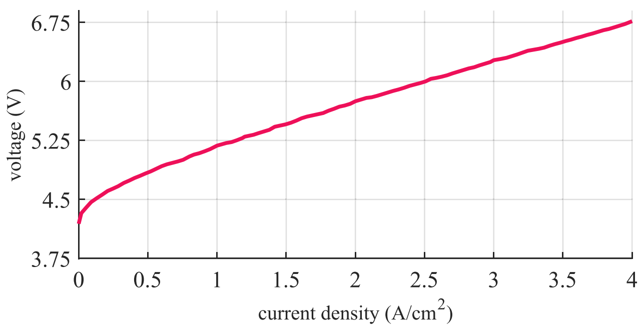

Fig. 3. Polarization curve of a generic commercial electrolyzer.

The actual cell voltage V is therefore:

$$V = E + V_{act} + V_{ohm} + V_{diff} \ , \tag{2}$$

where V_{act}, V_{ohm}, and V_{diff} represent the activation, ohmic, and diffusion overvoltages, respectively.

The static voltage–current characteristic derived from Eq. (2) is known as the polarization curve. An example of a commercial electrolyzer stack is shown in Fig. 3, where the diffusion-loss region is omitted as it lies beyond the rated operating range. Since the voltage of a single cell is typically only a few volts, multiple cells are connected in series to form a stack, making electrolyzers low-voltage, high-current loads.

Electrolyzer technologies differ mainly in the electrolyte material and can be classified into low and high-temperature systems. Low-temperature technologies include:

1. *liquid alkaline*, a mature and low-cost technology with high reliability, but limited dynamic performance and relatively low efficiency [35];
2. *proton exchange membrane (PEM)*, characterized by high efficiency, high current density, and good dynamic response, although it relies on expensive rare materials [36];
3. *anion exchange membrane (AEM)*, an emerging technology combining some advantages of alkaline and PEM systems, but still affected by durability and performance limitations [37].

High-temperature electrolyzers mainly consist of solid oxide (SO) systems, which offer higher efficiencies but require greater system complexity, have long start-up times, and remain costly due to their lower technological maturity [38,39].

Among these technologies, alkaline and PEM electrolyzers are the most widely adopted in PV-powered hydrogen production systems. For PEM electrolyzers, current ripple has been shown to reduce both conversion efficiency [40,41] and cell lifetime [42]. Consequently, minimizing current ripple is essential to improve durability and reduce system costs.

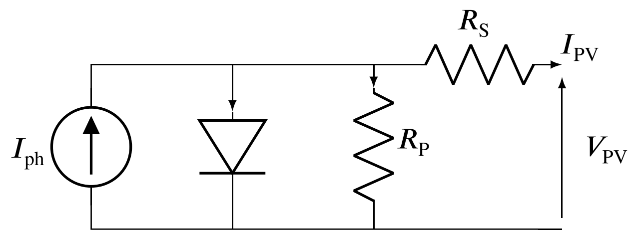

Fig. 4. Circuit diagram of the single diode model of a PV cell.

2.2. Photovoltaic characteristics

The electrical behaviour of a PV generator can be described using either the single-diode or double-diode model [43]. Among these, the single-diode model is the most widely adopted due to its simplicity and ability to accurately represent PV characteristics. Its equivalent circuit is shown in Fig. 4.

Due to the non-linear behaviour of the diode, the PV generator also exhibits a non-linear voltage–current characteristic. By applying Kirchhoff's Current Law to the equivalent circuit, the following expression can be obtained [44,45]:

$$I_{PV} = I_{ph} - I_0 \left[exp\left(\frac{q(V_{PV} + R_S I_{PV})}{AkT} \right) - 1 \right] - \frac{V_{PV} + R_S I_{PV}}{R_P} \ , \tag{3}$$

where I_{ph} is the photocurrent, I_0 is the diode reverse saturation current, q is the electron charge, R_S and R_P are the series and parallel resistances, A is the diode ideality factor, k is Boltzmann's constant, and T is the absolute temperature. Since R_S is typically very small and R_P very large, their effects can often be neglected, leading to a simplified form of Eq. (3):

$$I_{PV} = N_P \left[I_{ph} - I_0 exp\left(\frac{qV_{PV}}{N_S AkT} \right) - \frac{V_{PV}}{N_S} \right] \ . \tag{4}$$

As shown by Eqs. (3) and (4), the electrical characteristics of PV systems are strongly influenced by environmental conditions, particularly temperature and solar irradiation. Fig. 5 illustrates, as an example, the voltage–current and power characteristics of a generic PV panel under different operating conditions. Variations in irradiation can significantly affect both the output voltage and current, leading to substantial changes in the available power. For this reason, converters interfacing PV panels must implement a maximum power point tracking (MPPT) algorithm to ensure optimal energy extraction [44–46].

Several MPPT algorithms have been developed, the most common being Perturb and Observe (P&O), Incremental Conductance (IC), Sliding Mode Control (SMC), and, more recently, Artificial Neural Networks (ANNs). The P&O method periodically perturbs the converter duty cycle and observes the resulting power variation, causing operation to oscillate around the MPP. It is simple and computationally inexpensive, but may fail under multiple-MPP conditions, such as partial shading. The IC

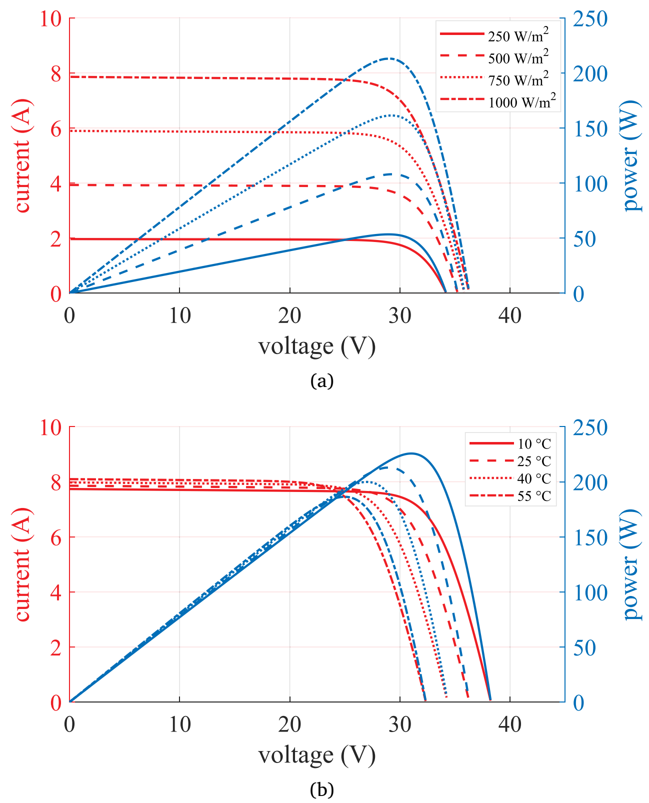

Fig. 5. Electrical characteristics of a generic PV panel based on different ambient conditions: (a) changing the irradiation, and (b) changing the temperature.

method uses voltage and current measurements to determine the power derivative and identify the MPP condition directly. It provides greater accuracy than P&O, although at the expense of increased implementation complexity. SMC is a non-linear control technique that defines a mathematical condition corresponding to MPP operation and forces the converter to satisfy it through a switching control law. This approach offers fast dynamic response and strong robustness to variations in irradiance, temperature, and system parameters, but requires a more sophisticated design. Finally, ANNs can be trained to estimate the MPP by considering multiple variables, such as irradiance, temperature, and seasonal effects. Although they require high-quality training data and greater computational resources, they are particularly effective under complex operating conditions and partial shading.

In recent years, the use of one converter per panel has become increasingly common, enabling more accurate MPPT and mitigating mismatch losses caused by partial shading [47,48]. Besides high efficiency and low cost, converters may also be required to regulate a constant output voltage despite variations in the PV input voltage, depending on the system application [45].

2.3. Converter characteristics

To summarize, considering that the electrolyzer is a low-voltage, high-current load, while PV systems are generally designed to have high voltages and low currents, the converters connected to the electrolyzer must have a step-down characteristic. To preserve the stack, another important feature is a high-frequency (in the order of tens of kHz) current ripple with low amplitude or, better still, no ripple at all. Other basic features sought in a stationary application are high efficiency, be economical, have high reliability (in case of power switch failures), and be able to perform MPPT. A further feature that may be required, but

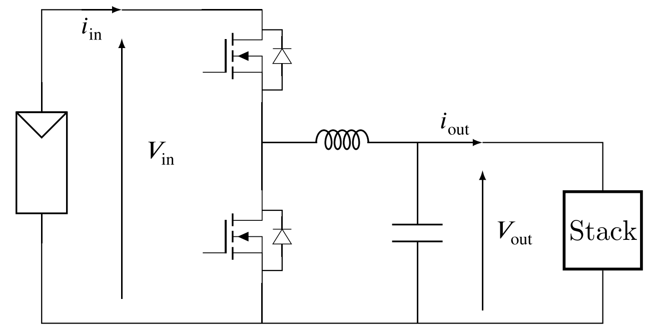

Fig. 6. Circuit scheme of a synchronous buck converter.

in stationary applications is not always necessary, is power density. In addition, galvanic isolation may not always be required, but in the case of grid integration, it may be necessary. Therefore, both isolated and non-isolated topologies can be considered, depending on the system requirements.

3. Non-isolated topologies

Non-isolated topologies are considered to be all those circuit topologies where there is no galvanic isolation between the power source and the load.

The simplest possible connection scheme between PV and electrolyzer (excluding the direct connection) is with a single converter. Depending on the voltage characteristics of the source and load, this could be a buck or boost converter. In most studies, a buck converter is considered because, as already mentioned, the stack is a low-voltage load. In some studies, the considered topology is not specified in detail [49,50], but in the majority of studies employing a single converter, an asynchronous buck is considered.

3.1. Asynchronous and synchronous buck

In [51], a mathematical model of the system is developed, considering a 500 kW plant and using a classic P&O algorithm as the control strategy for MPPT. Similarly, in [52], the P&O algorithm is adopted as the control method, but the case study focused on a 7 kW plant. Other works that employ P&O as the control algorithm include [53,54], although the power levels considered in these studies are much lower. In [55], a small-scale setup (2 W) is implemented, aiming to provide a constant voltage to the load. In [56], a 5 kW electrolyzer is analysed, with the control once again designed to ensure a constant output voltage. In [57], rather than focusing primarily on mathematical modelling, the emphasis is placed on converter control, specifically through the adoption of a SMC algorithm. In [58,59], the IC method is applied for MPPT, in systems rated at 250 W and 1.5 kW, respectively. In [60], a 7.8 kW electrolyzer integrated into a system including additional storage technologies is considered. In this case, the PV array is directly connected to the DC bus, and the overall system control is based on a modified invasive weed optimization combined with P&O. Finally, [61] also investigates a hybrid storage system, with the PV array directly connected to the DC bus and an electrolyzer rated at 50 kW.

In Fig. 6, the circuit diagram of a synchronous buck converter is reported. The asynchronous version could be obtained by removing the lower switch while preserving only the diode. This is a basic topology, which theoretically allows the mean value of the output voltage V_{out} to be adjusted between 0 and the supply voltage V_{in}, as in:

$$V_{out} = DV_{in} , \tag{5}$$

where D is the duty cycle. However, the input current is impulsive, while the output current is levelled by the presence of the inductor. The peak-to-peak output current ripple Δi_{Lpp} can be calculated as:

$$\Delta i_{\mathrm{out,pp}} = \frac{V_{\mathrm{in}}}{L f_{\mathrm{sw}}}(1 - D)D \ . \tag{6}$$

Eq. (6) shows that the amplitude and frequency of the oscillations on the output current depend on the switching frequency f_{sw} and the chosen inductance L. The correct dimensioning of reactive components is therefore crucial to prevent damaging ripples on the electrolyzer.

Furthermore, if a synchronous converter is used, at low loads, due to the ripple, the current may assume negative values within the switching period. This is not necessarily a problem for the electrolyzer, as electrical dynamics are faster than mechanical ones, but it could be an explanation for preferring to consider asynchronous converters. Another advantage of asynchronous converters is the possibility of working naturally in boundary condition mode (BCM), thus being able to reduce switching losses.

To partially circumvent the limitations of the single buck, cases where two asynchronous buck converters are cascaded have also been considered [62].

3.2. Asynchronous and synchronous boost

Rarer are the cases where a boost is considered as a converter. In these rare cases, both asynchronous [63–67] and synchronous [68] boosts topology are considered. In these cases, the situation is a mirror image of the buck. Theoretically, the output voltage of the converter can go from V_{in} to infinity, as in:

$$V_{\mathrm{out}} = \frac{V_{\mathrm{in}}}{1 - D} \ , \tag{7}$$

but in reality, this is not possible due to conduction losses in the components. So generally, the duty cycle is limited to prevent excessive losses and guarantee a correct operation of the converter. In addition, the current on the electrolyzer side will be discontinuous, while on the PV side it will be levelled by the inductor. This, however, is not ideal for the electrolyzer, which could be prematurely damaged. However, it is preferable for the PV as it can perform the MPPT more precisely. In [65,66,68], the P&O algorithm was selected for MPPT implementation, whereas the IC method was adopted in [67].

The use of a boost converter can be justified in PV systems where all panels are connected in parallel. In such a configuration, the minimum operating voltage of the electrolyzer stack may exceed the voltage of a single PV panel. However, since the arrangement of the PV panels is a design variable, this situation can generally be avoided by selecting an appropriate panel configuration. Given that the electrolyzer stack is typically the most expensive component of the system, it is preferable to adapt the PV layout rather than subject the stack to potentially unfavourable operating conditions.

3.3. Interleaved buck

A well-known option for reducing current ripple on the electrolyzer side is the use of interleaved topologies. In [69], a 500 W synchronous interleaved buck converter with 6 legs is considered, while in [70], an asynchronous one with 3 legs is coupled to a 5.6 kW electrolyzer. The circuit diagram of a generic synchronous interleaved buck converter with N legs is shown in Fig. 7. In general, these topologies have the same input–output characteristics as the buck converters already mentioned (as in Eq. (5)), but allow a reduction of the ripple on the output current by a factor proportional to the number of legs used. In certain operating points, it is also possible to completely eliminate the current ripple. This is achieved by a phase shift between the carriers of the gate signals.

In the synchronous interleaved buck, the output current is shared between all operating legs. The phase of each leg current is evenly

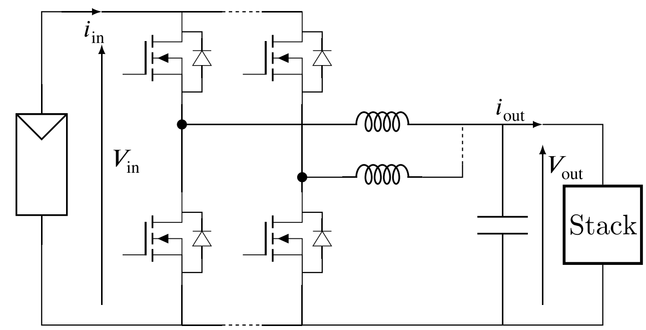

Fig. 7. Circuit scheme of a synchronous interleaved buck converter.

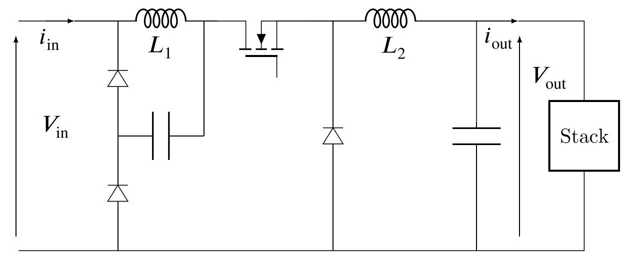

Fig. 8. Circuit scheme of a quadratic buck converter.

shifted by an electric angle equal to $360°/N$. The upper and lower switches of each leg operate in a complementary manner.

Eq. (8) expresses the peak-to-peak ripple pattern of the output current $\Delta i_{\mathrm{out,pp}}$ for any operating condition. It is basically a generalization of Eq. (6), considering N legs instead of 1:

$$\Delta i_{\mathrm{out,pp}} = \frac{V_{\mathrm{in}}}{L f_{\mathrm{sw}}}\left[1 - N\left(D - \frac{p-1}{N}\right)\right]\left(D - \frac{p-1}{N}\right) \ , \tag{8}$$

where p is the integer number obtained from:

$$p = \mathrm{ceil}(N D) \ . \tag{9}$$

As already mentioned before, based on Eqs. (8) and (9), with the interleaved topology, there are $N + 1$ duty cycles in which it is possible to obtain a zero input current ripple.

3.4. Quadratic buck

Another converter topology considered, similar to the standard buck already discussed, is the quadratic buck [57]. This topology differs in the presence of an additional circuit portion on the input. The circuit diagram of this topology is shown in Fig. 8. This provides an additional reduction in output voltage with the same duty cycle. In this case, the voltage input–output relationship of the converter is:

$$V_{\mathrm{out}} = D^2 V_{\mathrm{in}} \ . \tag{10}$$

However, this advantage is achieved, as already mentioned, by using more reactive components, thus increasing costs and losses compared to the standard buck. The equation describing the ripple of the converter output current in this case is [71]:

$$\Delta i_{\mathrm{out,pp}} = \frac{V_{\mathrm{in}}}{L_2 f_{\mathrm{sw}}}(1 - D)D^2 \ , \tag{11}$$

where L_2 is the inductance on the output port of the converter. The converter considered in this study is also an asynchronous one, so it has the advantage of operating in BCM.

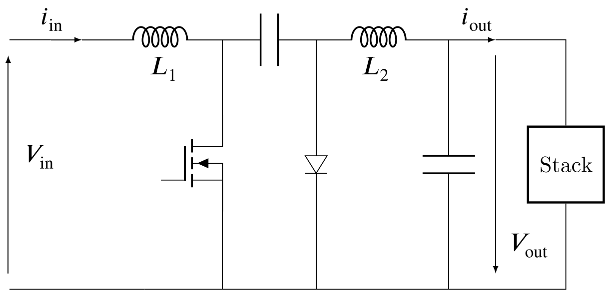

Fig. 9. Circuit scheme of the Cùk converter.

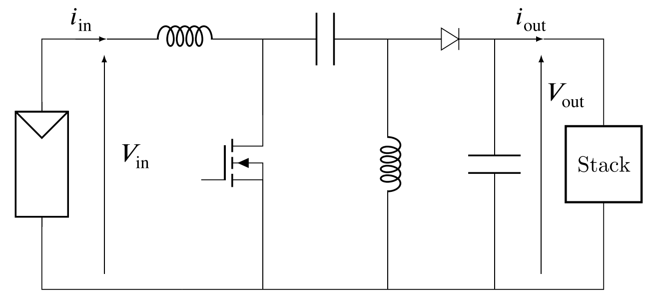

Fig. 10. Circuit scheme of the SEPIC converter.

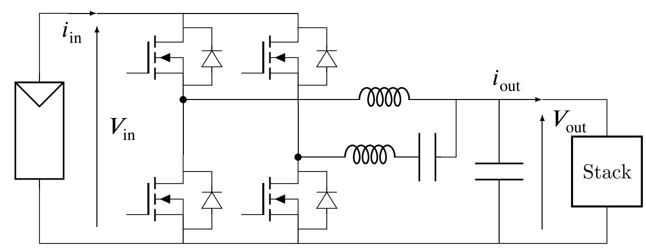

Fig. 11. Circuit scheme of a stacked interleaved buck converter.

3.5. *Cùk*

Other known topologies considered in the connection of PV and electrolyzer are the Cùk and Single-Ended Primary-Inductor Converter (SEPIC) [72], which are reported respectively in Fig. 9 and in Fig. 10. The Cùk converter features improved current quality due to the presence of inductances on both the input and output. This makes it possible to implement both a precise MPPT and to subject the stack to continuous currents. Also, thanks to the diode, it can operate in BCM. The circuit diagram is shown in Fig. 9.

The voltage input–output relationship for this converter is:

$$V_{\text{out}} = \frac{D}{1-D} V_{\text{in}} \,. \tag{12}$$

From Eq. (12) it can be seen that this topology can act as both a buck and a boost, depending on whether D is less than or more than 0.5. In an application such as the one considered, however, once the PV system has been realized and the stack selected (and thus when the voltage ranges have been fixed), this implies limiting the duty cycle to a precise range. About the current ripple in this case, the ripple on the output current can be computed as:

$$\Delta i_{\text{out,pp}} = \frac{V_{\text{in}}}{L_2 f_{\text{sw}}} D \,, \tag{13}$$

where L_2 is the inductance on the output port of the converter. By exploiting the magnetic coupling between the inductors or using other variants of the Cùk, theoretically it is possible to achieve ripple-free on both output and input currents [73]. However, this increases the cost and design complexity of the converter. A further problem with this topology is the inversion of the polarity of the output voltage.

3.6. *SEPIC*

The SEPIC has characteristics similar to the Cùk but does not have the problem of output voltage inversion. Its input–output voltage characteristic is the same as the Cùk. Thus, SEPIC can also function as both a buck and a boost. However, this is at the expense of the quality of the output current, which becomes discontinuous as it is no longer levelled by an inductor. Its circuit diagram is shown in Fig. 10.

Both the Cùk and SEPIC require more components than the standard buck, as well as a worst-case switch and diode sizing. This is because when the switch and the diode are not conducting, they are subject to $V_{\text{in}} + V_{\text{out}}$, and when conducting, they are subject to $i_{\text{in}} + i_{\text{out}}$.

In [72], several control algorithms for both converters are compared. The P&O method is evaluated against a control strategy based on ANNs, showing that the latter achieves higher accuracy, albeit with greater computational complexity.

3.7. *Stacked interleaved buck*

Another topology considered for this type of application is the stacked interleaved. In [74], to power a 400 W electrolyzer, a stacked interleaved synchronous buck is considered. Its circuit diagram is shown in Fig. 11. This converter resembles a synchronous interleaved buck with two legs, but differs in that it has a capacitor in series with the inductor on one of the legs (called the cancellation leg). This allows the continuous component of the current to be blocked and only the ripple to pass through. By operating it in such a way that the ripple on the cancellation leg is in phase opposition to that on the other leg, total cancellation of the current ripple on the output can be achieved for any operating point. This is an advantage for the stack, but the input current remains discontinuous, as in the case of the buck. For the converter control in [74], a dual closed-loop strategy is implemented, aiming to achieve an output voltage equal to a given reference input.

3.8. *Non isolated grid-connected configurations*

In the majority of studies done, the system is considered to be off-grid. In this way, all the energy produced by the PV flows directly to the electrolyzer. The control logic studied, therefore, focuses solely on the maximum transfer of energy from the source to the electrolyzer to maximize hydrogen production. The few cases with only one converter used for the PV or the electrolyzer in which a grid connection is mentioned or considered are those that involve greater plant engineering complexity, i.e. where other components are also integrated, such as fuel cells or batteries [59–61,65,66]. In these cases, the PV is connected directly to the DC bus, and the converter is used to power only the electrolyzer, as the MPPT is done by adjusting the DC bus voltage.

The second case most frequently considered in the various studies is the one with one converter for the PV and one for the electrolyzer, as shown in Fig. 2(b). In this case, there is greater variability in topologies, as different combinations of converters are possible. Generally, in this system configuration, a converter with a boost characteristic for the PV and a buck characteristic for the electrolyzer is almost always considered [75–78].

In some cases, the topology considered for one of the two converters is not specified [79–84], because the focus could be more on the load, or more on the generator, or more generally on the energy management of the system. However, the most considered topologies remain the asynchronous boost for the PV and the asynchronous buck for the electrolyzer [85–90]. In some special cases, converters of the same type are considered for both PV and electrolyzer: generic boost [91],

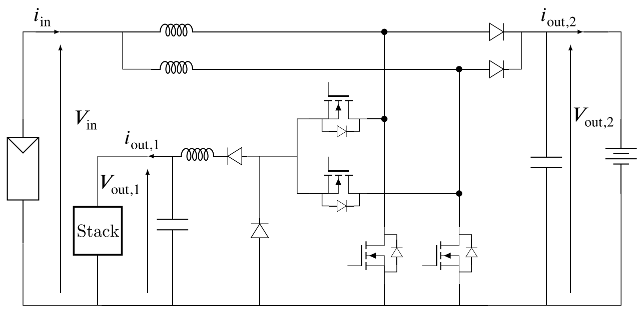

Fig. 12. Circuit scheme of the multi-port converter presented in [95].

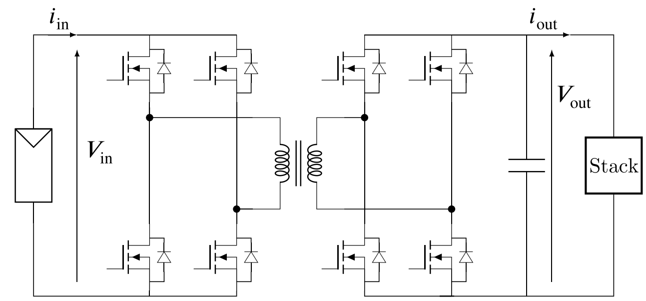

Fig. 13. Circuit scheme of the DAB converter.

asynchronous buck [92], or 3-leg synchronous interleaved buck [93]. In one case [94], an asynchronous boost is considered for the PV, and a stacked interleaved buck is considered for the electrolyzer.

The pros and cons of the various converter topologies have already been discussed. The use of dedicated converters is mainly related to the fact that they are considered in more complex systems consisting of more than just PV and electrolyzer. Generally, microgrids with loads and other storage systems, such as batteries, are considered. In most cases, these microgrids are considered to work off-grid, but integration with the grid is also considered in some cases. The use of dedicated converters allows for disconnected management of the individual components, thus allowing, for example, the electrolyzer to work at the point of maximum efficiency while the PV follows its own MPPT. This could not be possible without the use of various storage systems, such as batteries or grid integration, to compensate for power differences. Thus, despite the presence of multiple conversion stages, systems of this type allow greater flexibility by distributing energy flows more rationally. Converter control techniques may also vary depending on the purposes of the studies or the applications considered; there is no standard. In general, the converter connected to the PV performs some type of MPPT, while the one connected to the electrolyzer operates either to obtain a fixed production quota of hydrogen or to store excess energy.

3.9. Non isolated multi-port converter

A special case to be mentioned, which combines what has been said so far, is the use of multi-port converters. These topologies allow several components to be integrated via the same converter, such as PV, batteries, and electrolyzer.

At the moment, there is only one paper that proposes a specific non-isolated topology designed for this kind of application [95]. In this article, the authors propose a non-isolated three-port converter integrating a PV system, a PEM electrolyzer, and a generic DC bus. The circuit diagram of this topology is shown in Fig. 12. The converter operates as a boost towards the DC bus and as a buck towards the stack. The converter's control logic is based on meeting the power demand of the DC bus, to which a load or another storage system may be connected, and transferring only the excess power that would not be absorbed by the DC bus to the electrolyzer. In this manner, the converter operates to perform MPPT and activates the stack power supply only when excess power is present.

4. Isolated topologies

Isolated topologies include all those topologies with some type of galvanic isolation inside. Galvanic isolation is usually realized by means of high-frequency transformers, which make it possible to reduce volumes compared to low-frequency transformers. This is particularly important in high-power applications such as large electrolyzers. In this category of converters, the voltage input–output relationship of each converter will depend on the number of windings n of the transformer used. In general, there is therefore greater flexibility in the choice of conversion ratios, and it is not limited by the duty cycle as in non-isolated topologies. Again, there may be studies in which a system consisting only of PV and electrolyzer is considered, and others in which a microgrid is considered. In some studies, the exact topology is not specified, but they refer to isolated topologies [96,97].

4.1. Dual active bridge

When considering a system consisting only of PV and stack, a well-known isolated converter topology that is considered is the dual active bridge (DAB) [98,99]. The power of the case studies considered for the application of DAB ranges from 2.9 MW in [98] to 80 kW in [99]. The DAB consists of two H-bridges separated by a transformer, as shown in Fig. 13. Power transfer is achieved by the relative phase shift between the two H-bridges. Depending on the relative phase shift between the two, the power flow can be in one direction or the other. It is therefore a bidirectional converter, although this feature is not useful for the application under consideration. The relationship between input and output in a DAB converter therefore depends on the duty cycles of both H-bridges (D_1 and D_2) and the relative duty cycle between the two (D_0) as reported in [99]:

$$V_{out} = \frac{\sin\left[\frac{\pi}{2}(1-D_1)\right]\sin\left(2\pi f_{sw}t - \frac{\pi}{2}D_1\right)}{\sin\left[\frac{\pi}{2}(1-D_2)\right]\sin\left[2\pi f_{sw}t - \pi\left(D_1 + D_0 - \frac{D_2}{2}\right)\right]}\,. \tag{14}$$

In [99], the effect that the three-phase shift modulation used to control the DAB has on current ripple is also analysed. It is shown that to perform the MPPT, which involves dynamic changes in the three shift ratios, results in oscillations in the equivalent impedance on the primary side of the DAB converter. This leads to poor adaptability to photovoltaic fluctuations when connected to the PEM electrolyzer, causing an increase in the output current ripple.

4.2. Push–pull

Another isolated converter topology considered is the full bridge followed by a push–pull topology, as studied in [100], with a case study of a 19 kW system. The scheme described is illustrated in Fig. 14. This converter offers bidirectional power flow, but in this application, it is unwanted. Additionally, it features soft switching operation for all semiconductor components over a wide range of input power and voltage. In [100], unlike other cases already discussed, the converter is not designed to perform MPPT, but only to operate the electrolyzer at a fixed operating point. Thus, it works to the detriment of the PV, which will lead to it working less efficiently.

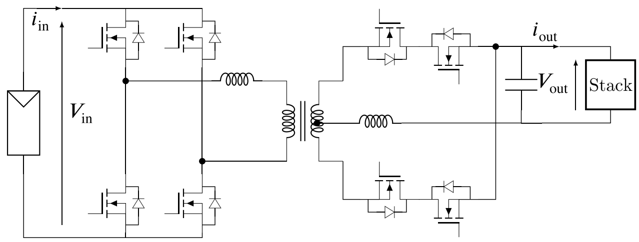

Fig. 14. Circuit scheme of a full bridge at primary and a push–pull at secondary.

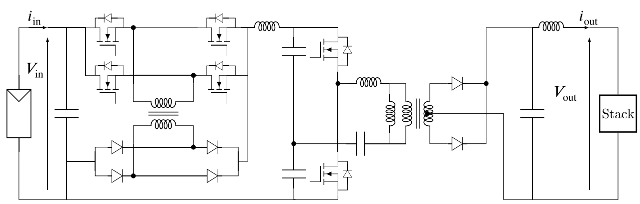

Fig. 15. Multi-stage LLC resonant converter with partial power processing converter followed by a half-bridge at primary and a centre tapped at secondary.

4.3. Resonant converters

Another macro category of isolated converters is the resonant converters. Along with the high-frequency transformer, these topologies also feature a stage of reactive components connected in a way that creates a resonant system at a precise frequency. The input–output relationship of these topologies can be seen as the product of three contributions: the inverter bridge gain, the transformer conversion ratio n, and the resonant tank gain K [101]. K is a coefficient that depends on converter design parameters, such as the various resonant components and the ratio of switching frequency to resonance frequency.

Several studies have considered isolated resonant topologies for connecting PV and electrolyzers. Particularly in these cases, there is a tendency to consider several converters connected in series, even for systems consisting only of PV and a stack. This is a substantial difference from non-isolated topologies, where the use of multiple converters is only considered for more complex systems, such as microgrids. These architectures will be referred to as multi-stage converters. In [102], two different two-stage converter topologies are compared for a 5.5 kW case study, where the difference lies in the topology of the first stage. In one case, the first stage is a topology designed for partial power processing. While in the other, the first stage is a 2-leg asynchronous interleaved buck. In both cases, as a second stage, an LLC resonant half-bridge at primary and a centre-tapped at secondary is considered. Also, for both cases, a P&O MPPT algorithm is considered to control the converter. The circuit diagrams of the two cases considered are shown respectively in Fig. 15 and Fig. 16(a).

However, the focus of the article is on the overall efficiency of the converter, so a comparison of the current quality on the stack is lacking. It has been shown that at low loads the system with the partial power processing stage has a higher efficiency. This advantage, however, is achieved at the expense of more components, including a second high-frequency transformer.

In [101] instead, four different isolated two-stage topologies are compared for a 5 kW case study. The first stage considered is always an asynchronous interleaved buck; what changes is the second stage. In the first case, an LLC resonant H-bridge on the primary side and a diode rectifier on the secondary is considered as the isolated converter, as shown in Fig. 16(b). In the second case, it is considered the same H-bridge at primary and a centre-tapped at secondary, the diagram of which is shown in Fig. 16(c). The third case involves an LLC resonant half bridge at the primary and a diode rectifier at the secondary (Fig. 16(d)). The last case is the same as the second one already dealt with in [102] and reported in Fig. 16(a).

In this study, the objective behind the use of multi-stage converters is to be employed as a single power module of a multiple interleaved multistring PV system connected to a single high-power electrolyzer. The first stage acts as a pre-regulator and always performs the MPPT, while the second stage performs voltage matching (in this application voltage reduction) and provides galvanic isolation. Also in this paper, the focus is mainly on efficiency, and it is verified that centre-tapped topologies in the second conversion stage perform better in this respect.

The input–output voltage relation of the second stage considered in the various resonant converters already considered can be divided into two different groups: where there is an H-bridge, the inverter bridge gain is equal to 1, so the conversion ratio is

$$V_{out} = V_{in} n K \ , \tag{15}$$

while in the case the second stage is made with a half bridge, the inverter bridge gain is equal to 1/2, so the conversion ratio is

$$V_{out} = \frac{1}{2} V_{in} n K \ . \tag{16}$$

In [103], a topology similar to that seen in Fig. 16(b) is used for a 10 kW electrolyzer, except that the stages are reversed: the resonant H-bridge stage and the subsequent rectifier are connected to the PV, while the 2-leg interleaved buck is connected to the electrolyzer. The difference lies in the use of a synchronous topology for the interleaved.

In contrast, in [104] a converter is considered as in Fig. 16(b), but removing the first stage, so considering only the isolated resonant converter. The focus of the work is the comparison of different resonant tank configurations, showing that of all the various configurations, the LLC resonant tank is the one best suited for a 250 W electrolyzer application. This is because it guarantees lower switching losses and higher efficiency compared to the other configuration.

In [105], the multi-stage topology considered consists of an asynchronous buck to perform the MPPT with a P&O algorithm, followed by a phase shift full bridge centre tapped to connect to a 10 kW stack. The circuit diagram of this topology is shown in Fig. 17.

Even for isolated converters, when considering more complex systems, there may be cases where separate converters are used for each component or multi-port converters are employed. As with non-isolated topologies, in microgrids in which both PV and electrolyzer have dedicated converters, the topologies of both converters are not always shown. For example, as in [106], the converter topology responsible for performing the MPPT is not specified, while a full bridge is used for the electrolyzer at the primary and a double current rectifier at the secondary.

In [107], an asynchronous boost is used as a converter for the PV, while for the electrolyzer, the topology shown in Fig. 18 is considered. As a case study, a 1.5 MW plant is used for simulations. The task of the boost is always to perform the MPPT (in this case, using the IC algorithm), while the isolated converter regulates the voltage on the stack. In the specifics of this work, an extra storage system is not considered in parallel with the electrolyzers, so the DC bus voltage is free to vary as a result of PV power variations. This certainly preserves the stack, as it does not subject it to immediate and sudden power variations, but it does require an oversizing of the capacitors connected to the DC bus.

4.4. Isolated multi-port converters

In [108], a 500 W multi-port topology specifically designed for the integration of PV, batteries, and electrolyzer is proposed. Its circuit diagram is shown in Fig. 19(a). On the primary side of the circuit is an H-bridge, which acts as a synchronous interleaved buck to the battery

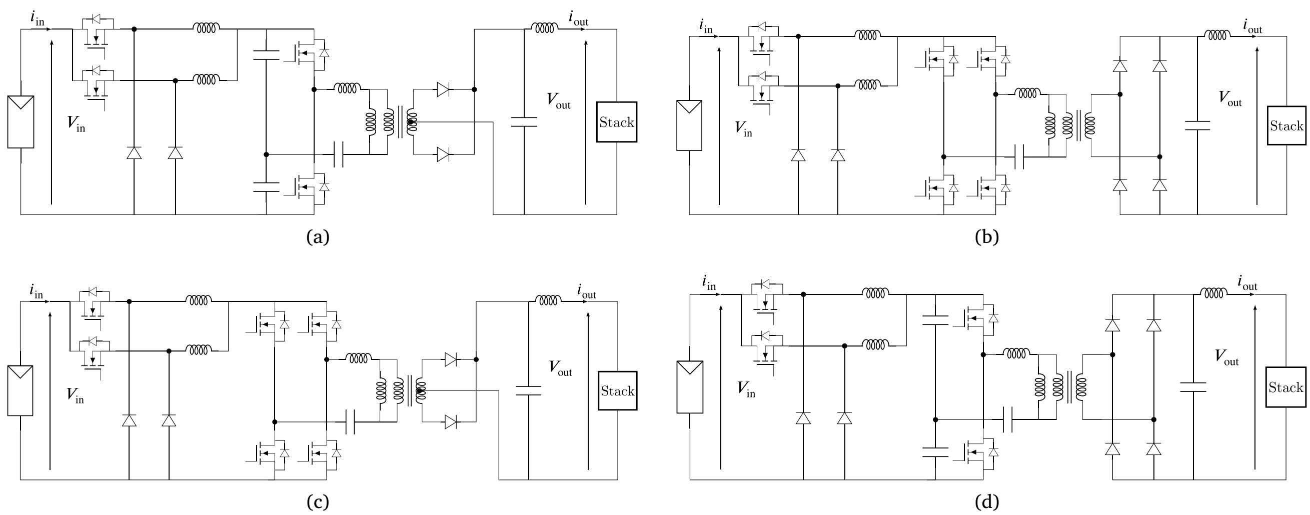

Fig. 16. Different types of multi-stage LLC resonant converter with interleaved buck converter as the first stage: (a) half-bridge at primary and centre tapped at secondary, (b) H-bridge at primary and diode rectifier at secondary, (c) H-bridge at primary and centre tapped at secondary, and (d) half-bridge at primary and diode rectifier at secondary.

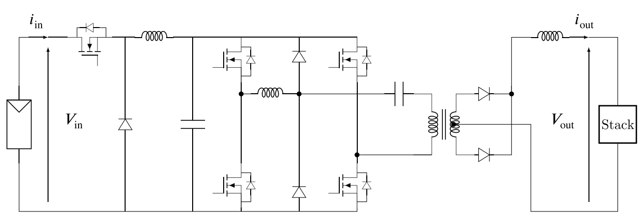

Fig. 17. Multi-stage converter composed of a buck converter and a phase shift full bridge.

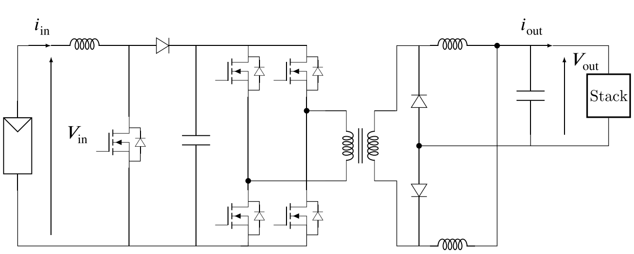

Fig. 18. Multi-stage converter composed of a boost converter and an isolated full bridge.

and as an LCC resonant converter to the stack. On the secondary side, on the other hand, there is an uncontrolled rectifier. The desired voltage on the port to which the battery is connected is obtained by the duty cycle computed from the MPPT, while that on the port to which the stack is connected is obtained by controlling the switching frequency. The relationship between the input voltage given by the PV and the output voltage on the stack can be written as:

$$V_{out} = \frac{V_{in}}{n}\frac{64 f_{sw}\sin(D\pi)}{K}, \tag{17}$$

where K is a coefficient that depends on converter design parameters, such as the ratio of the resonant capacitances, but also on the ratio of switching frequency to resonance frequency. This allows the operation of the PV and the stack to be controlled separately, thus being able to do the MPPT while the electrolyzer operates at a desired power. The current ripple on the stack with this topology is:

$$\Delta i_{out,pp} = \frac{V_{out}}{L_{out} f_{sw}}\left\{\frac{1}{2}\left[\cos\left(\arcsin\frac{2}{\pi}\right) - 1\right] + \frac{1}{\pi}\left(\arcsin\frac{2}{\pi}\right)\right\}. \tag{18}$$

Since the output voltage is mainly controlled by the switching frequency, the ripple of the current flowing through the stack in this case will depend less on the duty cycle.

In [109] instead, the multi-port configuration is achieved through a specially designed three-winding transformer. The converter is then realized through the use of three three-phase inverters, as can be seen in Fig. 19(b). The battery on the third port has been included for illustration purposes, but theoretically, it could also be the grid. The three-phase inverter is a well-known, elementary, and modular topology. Depending on the type of control, it could also be integrated into both off-grid and grid-connected systems. However, the design of a three-winding transformer may result in higher costs compared to two-winding transformers.

5. Discussion

For a more general discussion of the costs of the various topologies and their reliability, reference will be made to the number of components used. This is a simplification, since the reliability of a system depends on numerous factors, and it is not always the case that a greater number of components leads to a reduction in reliability [110–112]. Cost is also a simplification as some topologies, such as interleaved, allow the use of smaller components as the overall power can be spread evenly. Thus, the cost may not necessarily be proportional to the number of components. But the number of components can still provide a good estimate of the complexity of the single topology.

Table 1 therefore shows the number of components required for each topology treated. For interleaved topologies, the general case with N legs is always considered. When counting the components, all those listed in the circuit diagrams provided in the various studies under consideration are taken into account; therefore, where present and listed, components used as filters are also included. The only exception concerns the counting of diodes, where free-floating diodes and MOSFET's body diode have not been taken into account, as they may not be desired or may be directly integrated with the switch.

In addition, the Table shows the control techniques adopted for the different converter topologies, the power ranges considered for PV–electrolyzer applications, the reported converter efficiencies, and the type of validation performed, distinguishing between simulation-based and experimental studies.

In particular, the four-point efficiency is considered when evaluating converter performance. This metric is selected in order to assess

Table 1
Main characteristics of the various converters considered in this study.

Topology	Reference	Transformer	S/D/L/C	Control	Power range	Efficiency	Study type
Asynchronous buck	[51–61]	No	1/1/1/1	P&O, IC, SMC,Fixed V_{out}	2 W – 500 kW	N/A	Simulation and test with electrolyzer
Asynchronous boost	[63–67]	No	1/1/1/1	P&O, IC	1 – 200 kW	N/A	Simulation and test without electrolyzer
Asynchronous interleaved buck	[70]	No	N/N/N/1	SMC	5.6 kW	N/A	Simulation
Synchronous interleaved buck	[69]	No	2N/0/N/1	N/A	500 W	N/A	Simulation
Quadratic buck	[57]	No	1/3/2/2	SMC	330 W	N/A	Simulation
Cùk	[72]	No	1/1/2/2	P&O, ANN	N/A	N/A	Simulation
SEPIC	[72]	No	1/1/2/2	P&O, ANN	N/A	N/A	Simulation
Synchronous stacked interleaved buck	[74]	No	4/0/2/2	Fixed V_{out}	400 W	N/A	Simulation
Non-isolated multi-port	[95]	No	4/4/3/2	N/A	N/A	N/A	Simulation
DAB	[98,99]	Yes	8/0/0/1	N/A	80 kW – 2.9 MW	98.90%	Simulation
Full bridge/Push–pull	[100]	Yes	8/0/2/1	Fixed V_{out}	19 kW	N/A	Simulation and test without electrolyzer
Multi-stage with partial power processing	[102]	Yes	6/6/4/4	P&O	5.5 kW	98.26%	Simulation and test without electrolyzer
Multi-stage half-bridge/centre tapped	[101,102]	Yes	4/4/5/4	P&O	5 – 5.5 kW	99.23%	Simulation and test without electrolyzer
Multi-stage H-bridge/centre tapped	[101]	Yes	6/4/5/2	N/A	5 kW	98.90%	Simulation
Multi-stage H-bridge/diode rectifier	[101]	Yes	6/6/5/2	N/A	5 kW	98.32%	Simulation
Multi-stage half-bridge/diode rectifier	[101]	Yes	4/6/5/4	N/A	5 kW	98.45%	Simulation
Multi-stage with synchronous interleaved buck	[103]	Yes	8/4/3/4	N/A	10 kW	93.81%	Simulation and test with electrolyzer
H-bridge/diode rectifier	[104]	Yes	4/4/2/2	N/A	250 W	89.88%	Simulation
Multi-stage phase shift full bridge	[105]	Yes	5/5/3/2	P&O	10 kW	86.75%	Simulation and test with electrolyzer
Multi-stage asynchronous boost/isolated full bridge	[107]	Yes	5/3/3/2	IC	1.5 MW	N/A	Simulation
Isolated multi-port	[108]	Yes	4/4/4/4	Fixed V_{out}	500 W	89.25%	Simulation and test without electrolyzer
Isolated multi-port with 3 winding transformer	[109]	Yes	18/0/0/3	N/A	N/A	N/A	Simulation and test without electrolyzer

S = Switches; D = Diodes; L = Inductors; C = Capacitors.

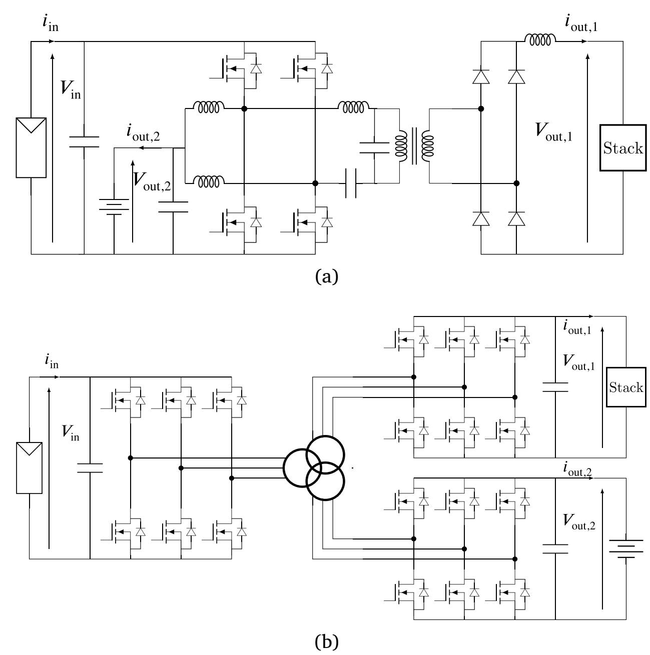

Fig. 19. Different types of isolated multi-port converter: (a) circuit scheme presented in [108], and (b) circuit scheme with the three-winding transformer presented in [109].

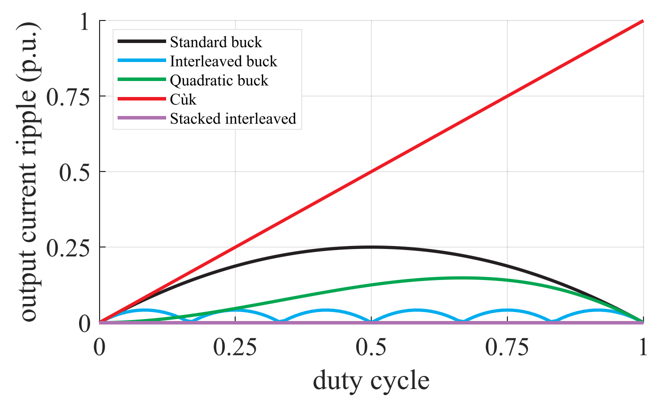

Fig. 20. Comparison of normalized output current ripple amplitude as a function of the duty cycle.

the efficiency of the converters across their entire intended operating power range. In some cases, however, it is not possible to determine this parameter, either because the efficiency is reported as a function of the converter operating time or because the relevant data are not provided. Where the available data points are insufficient for its calculation, the missing values are estimated through interpolation.

As can be seen from Table 1, for many topologies, the number of diodes to be used depends solely on whether or not an asynchronous topology is chosen. In general, for all those topologies in which an interleaved converter is present, the number of components depends on the number of legs. The topologies requiring a greater number of reactive components are the isolated resonant ones, where these are used to realize the resonant tank. Even among non-isolated topologies, some require extra reactive components, but these are still fewer in quantity than those required in isolated resonant topologies. Thus, it is realistic to assume that the isolated resonant topologies considered so far for PV hydrogen production are the most expensive and voluminous, not only because of the presence of the transformer.

Another aspect that can be noted from Table 1 is that, when specified, the gate signal generation systems primarily used in this type of application are based on well-known and established MPPT algorithms, such as P&O and IC. There are a few cases in which more complex algorithms, such as ANNs, are used.

Below is a comparison of the current ripple versus the duty cycle for the various topologies for which a formula was found, and for each of them, to obtain a normalized comparison, the same switching frequency, input voltage, and inductance values are considered. Topologies in which the current on the load is not levelled are not taken into account in this comparison, as they are considered the worst case regardless. As discussed above and as can be seen in Fig. 20, some topologies offer duty cycles in which the ripple cancels out. The best case here is the stacked interleaved buck. The quadratic buck performs better than the standard buck over the entire duty cycle range, and for low duty cycles even better than the 6-leg interleaved buck. As for the Cùk, on the other hand, it must be remembered that once the components and voltage levels have been chosen, its duty cycle range is limited to either 0 – 0.5 or 0.5 – 1, depending on whether it is used as a buck or a boost.

The interleaved buck converter offers an excellent compromise between ripple reduction, component count, and suitability for large-scale PV-hydrogen systems. Its modular structure makes it readily scalable to high-power applications, while increasing the number of phases inherently reduces the current ripple seen by the electrolyzer stack.

Compared with the stacked interleaved buck, it requires fewer components, resulting in higher efficiency and a simpler control scheme. Although it cannot inherently guarantee ripple-free operation over the entire operating range, it can be designed to operate at ripple-free points, partially overcoming this limitation while retaining its advantages in terms of simplicity and efficiency. Furthermore, the interleaved buck converter is suitable for a very wide range of applications, thanks to its simplicity and scalability. It can be used in high-voltage applications thanks to configurations such as series-input, parallel-output.

The suitability of each converter topology depends primarily on the required voltage conversion ratio, system power level, and isolation requirements. Non-isolated topologies are generally preferred when the PV array and electrolyzer stack operate at compatible voltage levels, as they offer lower cost and reduced complexity. Consequently, they are the most widely adopted solutions in both standalone PV–electrolyzer systems and larger microgrid architectures.

Isolated topologies become advantageous when a large voltage conversion ratio is required or when galvanic isolation is mandated by safety, regulatory, or system-integration constraints. The presence of a high-frequency transformer provides greater design flexibility and facilitates the interfacing of low-voltage, high-current electrolyzers with higher-voltage PV systems. However, this benefit comes at the expense of increased component count, cost, and control complexity.

With regard to power range, single-stage converters are generally preferred for low- and medium-power applications because they maximize overall conversion efficiency. Multi-stage and isolated solutions are more commonly considered in high-power installations, particularly when implemented as modular power-processing units within interleaved multi-string PV systems supplying a single large electrolyzer stack.

The challenges still facing the various types of converter certainly relate to testing on real systems, as most of the converters considered in this review have only been simulated or tested without an actual electrolyzer. The Cùk should be tested by trying out the design in which the magnetic circuit cancels the output ripple. Converters such as the H-bridge/diode rectifier and the multi-stage phase-shift full bridge require an improvement in efficiency, as they are currently below standard.

Beyond efficiency and dynamic performance considerations, the impact of power electronic converters on PEM electrolyzer durability deserves particular attention. Converter-induced current ripple and transient operating conditions may generate additional electrochemical and thermal stresses within the electrolyzer as reported in [113,114]. Depending on their amplitude and frequency content, these perturbations can affect catalyst degradation, membrane ageing, and overall system reliability [40–42]. Although several studies have reported that properly designed converters can limit these effects through suitable filtering and control strategies [115–117], the long-term relationship between converter operation and electrolyzer degradation remains an active research topic. Further investigations are therefore required to establish quantitative links between converter characteristics, current ripple, and electrolyzer lifetime under realistic renewable energy operating conditions.

It should be noted that, despite the growing interest in PEM electrolyzer durability under dynamic operating conditions, experimental investigations specifically addressing membrane degradation induced by converter-generated current ripple remain scarce. To date, the work of Parache et al. [42,113] constitutes one of the few dedicated studies on this topic, highlighting degradation effects mainly associated with increased high-frequency resistance and titanium porous transport layer deterioration rather than explicitly identifying membrane degradation mechanisms.

6. Future trends in PV-hydrogen system

6.1. Topology improvement

A first option for future improvement is the development of more partial power processing topologies for PV–electrolyzer applications. This allows more efficient management of the power produced, avoiding unnecessary dissipation in semiconductor devices. At present, what has already been studied [102] involves the use of two-stage converters. These two-stage topologies make use of a high-frequency transformer, whereas another recent study [118] has proposed a non-isolated partial power processing converter topology. One of the key issues that remain unresolved for many partial power processing topologies is the harmonic distortion imposed on the load. However, if this limitation will be overcome through the development of new and innovative topological designs, very high conversion efficiencies could potentially be achieved without compromising the lifetime of the load.

6.2. Modularity

The second aspect on which there could be future improvement is the use of multi-stack architectures or modular converters. The use of multi-stack system architectures has already been studied in applications where the renewable source is wind power [119,120]. Similarly, this concept could be extended to PV systems. Some studies have begun to investigate multi-stack systems connected to PV generation plants [115,116]. These architectures allow power to be distributed over several stacks, which enables the distribution of utilization and, consequently, stress. This also allows for studying strategies to improve the reliability of the system over the long term.

In addition to multi-stack architectures, another option could also be modular converter architectures, both series and parallel. There are already studies for these applications: in [121], a modular multilevel converter type π single-phase (π-MMC 1ph) was studied, while in [122], a modular multilevel converter is used to perform the MPPT, as each converter module is associated with a single PV panel, but the connection to the electrolyzer was not specified. These architectures would therefore also allow better utilization of the PV, as the problems of partial shading that occur in classical architectures with a single converter could be overcome.

6.3. New semiconductor technology

The last aspect to be considered for possible future developments is new semiconductor technologies, such as SiC, GaN, and diamond semiconductors. At present, the costs for some of these technologies are still very high. This does not make them attractive for applications with already high costs, such as those of a PEM stack. However, they could be of interest for this application in the future. The new materials used for semiconductors provide better conductivity, reducing conduction losses, better heat dissipation, and allow higher switching frequencies than classic silicon technology. The latter feature saves on the size of passive filters or transformers, helping reduce volume and costs. On the other hand, however, problems related to electromagnetic interference and related compatibility issues with other devices must be considered.

7. Conclusions

This article reviews the main converter topologies employed for coupling photovoltaic systems with electrolyzers for hydrogen production. The electrical characteristics of both PV generators and electrolyzer loads are first discussed in order to provide a comprehensive understanding of the system requirements and, consequently, of the fundamental features that the power converters must exhibit.

A wide range of converter topologies, both isolated and non-isolated, has been examined to offer a clear overview of the state of the art and of the solutions that have already been explored in the literature. With regard to non-isolated configurations, there is a strong reliance on well-established topologies such as buck and boost converters. In contrast, isolated solutions exhibit a significantly broader variety, largely due to the adoption of multi-stage architectures that allow greater flexibility in voltage adaptation and system integration.

The control strategies employed for system operation are also largely based on well-known algorithms, such as Perturb and Observe and Incremental Conductance. Nevertheless, despite the maturity of these approaches, the application of power electronics to PV-powered hydrogen production remains a rapidly evolving field.

In particular, there is still substantial potential for further development in areas such as non-isolated multiport topologies, the adoption of advanced semiconductor technologies, and the implementation of highly modular system architectures. These aspects represent promising directions for future research aimed at improving efficiency, scalability, and overall system performance.

CRediT authorship contribution statement

Paolo Pilati: Writing – review & editing, Writing – original draft, Visualization, Validation, Software, Project administration, Methodology, Investigation, Formal analysis, Data curation, Conceptualization. **Riccardo Mandrioli:** Writing – review & editing, Visualization, Validation, Methodology, Investigation, Formal analysis, Data curation. **Vincenzo Cirimele:** Writing – review & editing, Visualization, Validation, Methodology, Investigation, Formal analysis, Data curation. **Mattia Ricco:** Writing – review & editing, Visualization, Validation, Supervision, Project administration, Formal analysis. **Damien Guilbert:** Writing – review & editing, Visualization, Validation, Supervision, Project administration, Formal analysis, Conceptualization.

Declaration of competing interest

The authors declare that they have no known competing financial interests or personal relationships that could have appeared to influence the work reported in this paper.

References

[1] Houghton J. Global warming. Rep Progr Phys 2005;68(6):1343.
[2] Yolcan OO. World energy outlook and state of renewable energy: 10-year evaluation. Innov Green Dev 2023;2(4):100070.
[3] Farivar GG, Manalastas W, Tafti HD, Ceballos S, Sanchez-Ruiz A, Lovell EC, Konstantinou G, Townsend CD, Srinivasan M, Pou J. Grid-connected energy storage systems: State-of-the-art and emerging technologies. Proc IEEE 2022;111(4):397–420.
[4] Farias CBB, Barreiros RCS, da Silva MF, Casazza AA, Converti A, Sarubbo LA. Use of hydrogen as fuel: a trend of the 21st century. Energies 2022;15(1):311.
[5] Van Hoecke L, Laffineur L, Campe R, Perreault P, Verbruggen SW, Lenaerts S. Challenges in the use of hydrogen for maritime applications. Energy & Environ Sci 2021;14(2):815–43.
[6] Kumar SS, Himabindu V. Hydrogen production by PEM water electrolysis–a review. Mater Sci Energy Technol 2019;2(3):442–54.
[7] Dawood F, Anda M, Shafiullah G. Hydrogen production for energy: An overview. Int J Hydrog Energy 2020;45(7):3847–69.
[8] Salerno G, Cecconi B, Bettucci O, Monai M, Zani L, Franchi D, Calamante M, Mordini A, Montini T, Fornasiero P, et al. Enhanced long-term stability of a photosensitizer with a hydroxamic acid anchor in dye-sensitized photocatalytic hydrogen generation. Eur J Org Chem 2023;26(45):e202300924.
[9] Mohammadi A, Mehrpooya M. A comprehensive review on coupling different types of electrolyzer to renewable energy sources. Energy 2018;158:632–55.
[10] European Clean Hydrogen Alliance. Project pipeline of the European clean hydrogen alliance. 2022, URL https://single-market-economy.ec.europa.eu/industry/industrial-alliances/european-clean-hydrogen-alliance/project-pipeline_en.
[11] Kakoulaki G, Kougias I, Taylor N, Dolci F, Moya J, Jäger-Waldau A. Green hydrogen in Europe–a regional assessment: Substituting existing production with electrolysis powered by renewables. Energy Convers Manage 2021;228:113649.
[12] Hidaka Y, Kawahara K. Modeling of a hybrid system of photovoltaic and fuel cell for operational strategy in residential use. In: 2012 47th international universities power engineering conference. IEEE; 2012, p. 1–6.
[13] Kiaee M, Cruden A, Chladek P, Infield D. Demonstration of the operation and performance of a pressurised alkaline electrolyser operating in the hydrogen fuelling station in porsgrunn, Norway. Energy Convers Manage 2015;94:40–50.
[14] Pascuzzi S, Anifantis AS, Blanco I, Scarascia Mugnozza G. Electrolyzer performance analysis of an integrated hydrogen power system for greenhouse heating. a case study. Sustainability 2016;8(7):629.
[15] Wang X, Huang J, Xu Z, Zhang C, Guan X. Real-world scale deployment of hydrogen-integrated microgrid: design and control. IEEE Trans Sustain Energy 2024.
[16] Sayedin F, Maroufmashat A, Al-Adwani S, Khavas SS, Elkamel A, Fowler M. Evolutionary optimization approaches for direct coupling photovoltaic-electrolyzer systems. In: 2015 international conference on industrial engineering and operations management. IEEE; 2015, p. 1–8.
[17] Khalilnejad A, Sundararajan A, Sarwat AI. Performance evaluation of optimal photovoltaic-electrolyzer system with the purpose of maximum hydrogen storage. In: 2016 IEEE/IAS 52nd industrial and commercial power systems technical conference (i&cPS). IEEE; 2016, p. 1–9.
[18] Gaamouche R, Abbou A, Redouane A, El Hasnaoui A, Belhorma B. Modeling and simulation of direct coupling of an electrolyzer to pv system for hydrogen production. In: 2018 6th international renewable and sustainable energy conference. IEEE; 2018, p. 1–5.
[19] Azzolini JA, Tao M, Ayers K, Vacek J. A load-managing photovoltaic system for driving hydrogen production. In: 2020 47th IEEE photovoltaic specialists conference. IEEE; 2020, p. 1927–32.
[20] Solovey V, Zipunnikov M, Kotenko A. Researching and adjusting the modes of joint operation of a photoelectric converter and a high pressure electrolyzer. Int J Hydrog Energy 2022;47(66):28272–9.
[21] Kouache A, Djafour A, Benzaoui K, Gougui A, Danoune M, Ramdani M. Field investigation of green hydrogen production via indirect coupling of PEM electrolyzer in southeast Algeria. Int J Hydrog Energy 2024.
[22] Del Valle AG, García-Linares P, Martí A. Optimizing hydrogen production: A comparative study of direct and indirect coupling between photovoltaics and electrolyzer. Energy Convers Manage 2024;315:118751.
[23] Merahi F, Bouamama BO, Mekhilef S, et al. Bond graph modeling, design and experimental validation of a photovoltaic/fuel cell/electrolyzer/battery hybrid power system. Int J Hydrog Energy 2021;46(47):24011–27.
[24] Behera MK, Saikia LC. A novel resilient control of grid-integrated solar PV-hybrid energy storage microgrid for power smoothing and pulse power load accommodation. IEEE Trans Power Electron 2022;38(3):3965–80.
[25] Abdo M, Abdel-Rahman MA, Amer M, Helmy S. Harmonic domain model of a hybrid PV-hydrogen/FC-electrolyzer system for steady-state analysis. In: 2023 24th international middle east power system conference. IEEE; 2023, p. 1–6.
[26] Hassan A, Abdel-Rahim O, Bajaj M, Zaitsev I. Power electronics for green hydrogen generation with focus on methods, topologies, and comparative analysis. Sci Rep 2024;14(1):24767.
[27] Sánchez L, Reigosa D, Bilbao A, Peña-Gonzalez I, Briz F. Comparative analysis of power converter topologies for hydrogen electrolyzers. IEEE J Emerg Sel Top Power Electron 2024.
[28] Yodwong B, Guilbert D, Phattanasak M, Kaewmanee W, Hinaje M, Vitale G. AC-dc converters for electrolyzer applications: State of the art and future challenges. Electronics 2020;9(6):912.
[29] El Kattel MB, Praça PP, Mayer R, Lucio Berrehil el Kattel CdC, Bascopé RPT, Antunes FLM, de Jesus Cardoso Filho B. Overview of main electrolyzer technologies and power electronic converter topologies for enabling hydrogen production through water electrolysis. Int J Circuit Theory Appl 2024.
[30] Chen M, Chou S-F, Blaabjerg F, Davari P. Overview of power electronic converter topologies enabling large-scale hydrogen production via water electrolysis. Appl Sci 2022;12(4):1906.
[31] Guilbert D, Collura SM, Scipioni A. DC/DC converter topologies for electrolyzers: State-of-the-art and remaining key issues. Int J Hydrog Energy 2017;42(38):23966–85.
[32] Rego G, Rocha J, Faria JA, Afonso JL, Monteiro V. A review of hydrogen production methods and power electronics converter topologies for green hydrogen applications. Energies 2024;17(22):5579.
[33] Vitale G. Power converters for green hydrogen: State of the art and perspectives. Electronics 2024;13(22):4565.
[34] Marangio F, Santarelli M, Calì M. Theoretical model and experimental analysis of a high pressure pem water electrolyser for hydrogen production. Int J Hydrog Energy 2009;34(3):1143–58.
[35] David M, Ocampo-Martínez C, Sánchez-Peña R. Advances in alkaline water electrolyzers: A review. J Energy Storage 2019;23:392–403.
[36] Falcão D, Pinto A. A review on PEM electrolyzer modelling: Guidelines for beginners. J Clean Prod 2020;261:121184.
[37] Li C, Baek J-B. The promise of hydrogen production from alkaline anion exchange membrane electrolyzers. Nano Energy 2021;87:106162.
[38] Nejadian MM, Ahmadi P, Houshfar E. Comparative optimization study of three novel integrated hydrogen production systems with SOEC, PEM, and alkaline electrolyzer. Fuel 2023;336:126835.
[39] Ni M, Leung MK, Leung DY. Technological development of hydrogen production by solid oxide electrolyzer cell (SOEC). Int J Hydrog Energy 2008;33(9):2337–54.

[40] Buitendach HP, Gouws R, Martinson CA, Minnaar C, Bessarabov D. Effect of a ripple current on the efficiency of a PEM electrolyser. Results Eng 2021;10:100216.
[41] Järvinen L, Puranen P, Ruuskanen V, Kosonen A, Kauranen P, Ahola J, Chatzichristodoulou C. Experimental study of alkaline water electrolyzer performance and frequency behavior under high frequency dynamic operation. Int J Hydrog Energy 2024;67:50–61.
[42] Parache F, Schneider H, Turpin C, Richet N, Debellemanière O, Bru É, Thieu AT, Bertail C, Marot C. Impact of power converter current ripple on the degradation of PEM electrolyzer performances. Membranes 2022;12(2):109.
[43] Chin VJ, Salam Z, Ishaque K. Cell modelling and model parameters estimation techniques for photovoltaic simulator application: A review. Appl Energy 2015;154:500–19.
[44] Rajesh R, Mabel MC. A comprehensive review of photovoltaic systems. Renew Sustain Energy Rev 2015;51:231–48.
[45] Gopi RR, Sreejith S. Converter topologies in photovoltaic applications–a review. Renew Sustain Energy Rev 2018;94:1–14.
[46] Kasper M, Bortis D, Kolar JW. Classification and comparative evaluation of PV panel-integrated DC–DC converter concepts. IEEE Trans Power Electron 2013;29(5):2511–26.
[47] Jeong H, Lee H, Liu Y-C, Kim KA. Review of differential power processing converter techniques for photovoltaic applications. IEEE Trans Energy Convers 2018;34(1):351–60.
[48] Abdel-Rahim O, Chub A, Vinnikov D, Blinov A. DC integration of residential photovoltaic systems: A survey. IEEE Access 2022;10:66974–91.
[49] Omar FA. A new approach for improving the efficiency of the indirectly coupled photovoltaic-electrolyzer system. Int J Hydrog Energy 2023;48(24):8768–82.
[50] Sun Z, Peng Y, Zhang D. A control method based on improved cuckoo algorithm for photovoltaic hybrid hydrogen production system. In: 2024 the 9th international conference on power and renewable energy. IEEE; 2024, p. 1056–60.
[51] Zou L, Shen Q, Yang G, Li S, Huang N. Improved hydrogen production efficiency of a photovoltaic-electrolysis system with P&O algorithm: A case study. Chem Phys Lett 2023;832:140891.
[52] Awad M, Mahmoud MM, Elbarbary Z, Mohamed Ali L, Fahmy SN, Omar AI. Design and analysis of photovoltaic/wind operations at MPPT for hydrogen production using a PEM electrolyzer: Towards innovations in green technology. PLoS One 2023;18(7):e0287772.
[53] Kaddachi C, Harrabi R, Farhani S, Grissa H, Bacha F. Modeling and control of photovoltaic hydrogen production system. In: 2024 IEEE international conference on advanced systems and emergent technologies (iC_ASET). IEEE; 2024, p. 1–5.
[54] Farhani S, Kaddachi C, Bacha F. Study and simulation of green hydrogen production systems coupled with concentrated photovoltaic generators. In: 2024 IEEE international conference on artificial intelligence & green energy. IEEE; 2024, p. 1–5.
[55] Albarghot M, Rolland L. MATLAB/Simulink modelling and experimental results of a PEM electrolyzer powered by a solar panel. In: 2016 IEEE electrical power and energy conference. IEEE; 2016, p. 1–6.
[56] Harikrishnan A, Mehta P, Bharadwaj P. High performance switched moded power conversion for photovoltaic integrated hydrogen based energy system. In: 2023 IEEE 3rd international conference on smart technologies for power, energy and control. IEEE; 2023, p. 1–6.
[57] Mas R, Pichilingue D, Berastain A, Celis C. On the application of sliding mode control to indirectly coupled photovoltaic-electrolyzer systems used in the production of clean energy. Int J Thermofluids 2024;23:100747.
[58] Han Z, Yuan S, Wang J, Dong Y, Gao L, Yang Y. Modeling and control of photovoltaic hydrogen production system adapting to power fluctuations. In: 2021 IEEE 5th conference on energy internet and energy system integration (EI2). IEEE; 2021, p. 2835–40.
[59] Miron C, Christov N, Olteanu SC. Energy management of photovoltaic systems using fuel cells. In: 2016 20th international conference on system theory, control and computing. IEEE; 2016, p. 749–54.
[60] Pradhan C, Senapati MK, Malla SG, Nayak PK, Gjengedal T. Coordinated power management and control of standalone PV-hybrid system with modified IWO-based MPPT. IEEE Syst J 2020;15(3):3585–96.
[61] Gulzar MM, Iqbal A, Sibtain D, Khalid M. An innovative converterless solar PV control strategy for a grid connected hybrid PV/wind/fuel-cell system coupled with battery energy storage. IEEE Access 2023;11:23245–59.
[62] Xia Y, Cheng H, He H, Hu Z, Wei W. Efficiency enhancement for alkaline water electrolyzers directly driven by fluctuating PV power. IEEE Trans Ind Electron 2023;71(6):5755–65.
[63] El Amri M, Falama RZ, Saidi AS, Salah CB. Study of hydrogen production and storage PV system. In: 2022 IEEE 21st international ccnference on sciences and techniques of automatic control and computer engineering. IEEE; 2022, p. 528–32.
[64] Amri ME, Salah CB. Study of a PV/Battery system for hydrogen production and storage. In: 2022 IEEE 21st international ccnference on sciences and techniques of automatic control and computer engineering. IEEE; 2022, p. 522–7.
[65] Tlili N, Neily B, Salem FB. Modeling and simulation of hybrid system coupling a photovoltaic generator, a PEM fuel cell and an electrolyzer (part I). In: 2014 IEEE 11th international multi-conference on systems, signals & devices (SSD14). IEEE; 2014, p. 1–8.
[66] Tlili N, Neily B, Ben Salem F. Modeling and simulation of hybrid system coupling a photovoltaic generator, a PEM fuel cell and an electrolyzer (part II). In: 2014 IEEE 11th international multi-conference on systems, signals & devices (SSD14). 2014, p. 1–7. http://dx.doi.org/10.1109/SSD.2014.6808809.
[67] Hassan SZ, Mumtaz S, Kamal T, Khan L. Performance of grid-integrated photovoltaic/fuel cell/electrolyzer/battery hybrid power system. In: 2015 power generation system and renewable energy technologies. IEEE; 2015, p. 1–8.
[68] Lopez VM, Isabella O, Zeman M, Ziar H. Battery-less uncertainty-based control of a stand-alone PV-electrolyzer system. J Power Sources 2024;614:234934.
[69] Di Caro A, Vitale G. Direct-coupled improvement of a solar-powered proton exchange membrane electrolyzer by a reconfigurable source. Clean Technol 2024;6(3):1203–28.
[70] Koundi M, E.L. FADIL H. Mathematical modeling of PEM electrolyzer and design of a voltage controller by the SMPWM approach. In: 2019 international conference on power generation systems and renewable energy technologies. IEEE; 2019, p. 1–6.
[71] Rodríguez RAA, Moreno JAG, Castañeda LNR, Trujillo J. Modeling and simulation of a non-linear high-power quadratic buck converter from design analysis. Encuentro Int de Educación En IngenieríA 2023.
[72] Makhloufi AB, Hatti M, Taleb R. Comparative study of photovoltaic system for hydrogen electrolyzer system. In: 2017 6th international conference on systems and control. IEEE; 2017, p. 445–50.
[73] Cuk S, Middlebrook R. Advances in switched-mode power conversion part II. IEEE Trans Ind Electron 1983;(1):19–29.
[74] Makineni RR, Sutanto D, Muttaqi KM, Islam MR, Agalgaonkar AP. Dual loop cascade control of a stacked interleaved buck converter for electrolyzer application. In: 2022 IEEE IAS global conference on emerging technologies (globConET). IEEE; 2022, p. 1029–35.
[75] Iannuzzi D, Pagano M. Efficiency of hydrogen based storage systems for stand-alone pv applications: Numerical and experimental results. In: 2009 international conference on clean electrical power. IEEE; 2009, p. 555–61.
[76] Djoudi H, Badji A, Benyahia N, Zaouia M, Denoun H, Benamrouche N. Modeling and power management control of the photovoltaic and fuel cell/electrolyzer system for stand-alone applications. In: 2015 4th international conference on electrical engineering. IEEE; 2015, p. 1–6.
[77] Maaruf M, Khalid M. Hybrid solar/pem fuel cell/and water electrolyzer energy system for all-electric ship. In: 2022 IEEE kansas power and energy conference. IEEE; 2022, p. 1–5.
[78] Bayoumi MA, El Sayed F, Abdallah MG, Atallah AM, Hafez DM. Investigation of green hydrogen production and storage from PV arrays connected to an AC microgrid system. In: 2023 international telecommunications conference (ITC-Egypt). IEEE; 2023, p. 157–64.
[79] Rahman MM, Antonini G, Pearce JM. Open-source DC-DC converter enabling direct integration of solar photovoltaics with anion exchange membrane electrolyzer for green hydrogen production. Int J Hydrog Energy 2024;88:333–43.
[80] Palma L, Molina B, Díaz A. Design and sizing of power conversion system with energy storage for improved PV-electrolyzer energy coupling. In: 2023 international conference on clean electrical power. IEEE; 2023, p. 784–8.
[81] Agbossou K, Kolhe M, Hamelin J, Bose TK. Performance of a stand-alone renewable energy system based on energy storage as hydrogen. IEEE Trans Energy Convers 2004;19(3):633–40.
[82] Agbossou K, Kélouwani S, Anouar A, Kolhe M. Energy management of hydrogen-based stand-alone renewable energy system by using boost and buck converters. In: Conference record of the 2004 IEEE industry applications conference, 2004. 39th IAS annual meeting. 4, IEEE; 2004, p. 2786–93.
[83] Doumbia ML, Agbossou K, Granger E. Simulink modelling and simulation of a hydrogen based photovoltaic/wind energy system. In: EUROCON 2007-the international conference on“ computer as a tool”. IEEE; 2007, p. 2067–72.
[84] Doumbia ML, Agbossou K, Granger E. Modelling and simulation of a hydrogen based photovoltaic/wind energy system. In: 2007 IEEE international symposium on industrial electronics. IEEE; 2007, p. 2601–6.
[85] Kumar RK, Samuel P. Designing a hydrogen generation system through PEM water electrolysis with the capability to adjust fast fluctuations in photovoltaic power. Int J Hydrog Energy 2024;82:1–10.
[86] Dahmane N, Djerioui A, Zeghlache S, Dahmane ZE, Houari A, Hadjkaddour A. Energy management of PV/FC/BAT/SC and PEM electrolyzer. In: 2022 IEEE international conference on electrical sciences and technologies in maghreb. 4, IEEE; 2022, p. 1–6.
[87] Shaker FN, Obed AA, Abid AJ. Comprehensive design for a neuro-fuzzy controller for a safe hydrogen energy storage. In: 2022 10th international conference on smart grid (icSmartGrid). IEEE; 2022, p. 124–30.
[88] Kumar SS, Mukundan N, Jayaprakash P. Modified LMS control for a grid interactive PV–fuel cell–electrolyzer hybrid system with power dispatch to the grid. IEEE Trans Ind Appl 2022;58(6):7907–18.

[89] Zhong Y, Peng Y, Chen H, Hao G, Gao F, Zhou Z. An improved particle swarm optimization algorithm-based MPPT method for distributed photovoltaic hydrogen production systems. In: 2024 the 9th international conference on power and renewable energy. IEEE; 2024, p. 1091–6.

[90] Hossain MB, Islam MR, Muttaqi KM, Sutanto D, Agalgaonkar AP. A compensation strategy for mitigating intermittencies within a pv powered microgrid using a hybrid multilevel energy storage system. IEEE Trans Ind Appl 2023;59(4):5074–86.

[91] Bhosale R, Agarwal V. Control of fuel cell and electrolyzer based hydrogen storage system with ultra-capacitor for voltage stability and enhanced transient stability of a DC micro grid. In: 2018 international conference on power, instrumentation, control and computing. IEEE; 2018, p. 1–6.

[92] Liu X, Zou J, Long R, Liu Z, Liu W. Variable period sequence control strategy for an off-grid photovoltaic-PEM electrolyzer hydrogen generation system. Renew Energy 2023;216:119074.

[93] Rech TF, Orlando T, Coelho RF, Kirsten AL. Step-down converter for low current ripple in electrolyzer with mppt control strategy. In: 2023 IEEE 8th southern power electronics conference. IEEE; 2023, p. 1–7.

[94] Makineni RR, Agalgaonkar AP, Muttaqi KM, Islam MR, Sutanto D. Integral sliding mode control of a stacked interleaved buck converter for electrolyzers supplied with renewable energy sources. IEEE Trans Ind Appl 2024.

[95] Elbakly AM, Abdelsalam I, Marei MI. Interleaved multi-port non-isolated DC/DC converter for green hydrogen production with PV/PEM electrolyzer system. In: 2025 7th international youth conference on radio electronics, electrical and power engineering. IEEE; 2025, p. 1–5.

[96] Yonezawa Y, Atsushi M, Nakao H, Takauchi H, Nakashima Y, Ebe H, Yamashita D, Sugiyama M, Ota Y, Nishioka K. Model-based development of solar-to-hydrogen conversion system with dynamic operating point control of multiple DC-DC converters. In: 2018 7th international conference on renewable energy research and applications. IEEE; 2018, p. 1435–40.

[97] Yamashita D, Nakao H, Yonezawa Y, Nakashima Y, Ota Y, Nishioka K, Sugiyama M. A new solar to hydrogen conversion system with high efficiency and flexibility. In: 2017 IEEE 6th international conference on renewable energy research and applications. IEEE; 2017, p. 441–6.

[98] Geske M, Ablakovic D, Jalili K, Keller C. Direct coupling of solar plants and electrolyzers with voltage-source converters. In: 2024 IEEE sixth international conference on DC microgrids. IEEE; 2024, p. 1–8.

[99] Kang Z, Duan F. A flexible load adaptive control strategy for efficient photovoltaic hydrogen generation system. Sol Energy 2023;266:112150.

[100] Abdel-Rahim O, Arafa AA, et al. Efficient integration of pv panels and electrolysis through a high-performance converter for clean hydrogen generation. J Adv Res Appl Sci Eng Technol 2025;52(2):26–34.

[101] Concha D, Renaudineau H, Hernandez MS, Llor AM, Kouro S. Evaluation of DCX converters for off-grid photovoltaic-based green hydrogen production. Int J Hydrog Energy 2021;46(38):19861–70.

[102] Renaudineau H, Llor AM, Hernandez MS, Concha D, Wilson-Veas AH, Kouro S. Photovoltaic to electrolysis off-grid green hydrogen production with DC–DC conversion. Renew Energy 2024;237:121687.

[103] Kim K, Kim J-H, Lee J-P, Kim T-J, Oh C-Y. Converter design and control strategy for PEM water electrolyzer to increase hydrogen generation using hardware-in-the-loop simulation. In: 2024 IEEE applied power electronics conference and exposition. IEEE; 2024, p. 2960–4.

[104] Chandrasekhar P, Reddy SR. Performance of soft-switched DC-dc resonant converter for electrolyzer. In: 2011 4th international symposium on resilient control systems. IEEE; 2011, p. 95–100.

[105] Xiong J, Xia Y, Peng Y, Wei W. A multi-mode self-optimization electrolysis converting strategy for improving efficiency of alkaline water electrolyzers. IEEE Trans Power Electron 2023.

[106] Cavallaro C, Cecconi V, Chimento F, Musumeci S, Santonocito C, Sapuppo C. A phase-shift full bridge converter for the energy management of electrolyzer systems. In: 2007 IEEE international symposium on industrial electronics. IEEE; 2007, p. 2649–54.

[107] Yu T, Meng J, Xu Z, Xie H, Jia Z, Quan H. Modeling and simulation of photovoltaic off-grid hydrogen production system. In: 2022 international conference on environmental science and green energy. IEEE; 2022, p. 181–6.

[108] Li X, Li N, Xue W, Mao W, Qiu S, Wu X. LCC-resonant-type current-fed-out three-port DC–DC converter for PV electrolytic hydrogen production integrated with energy storage. IEEE Trans Ind Electron 2024.

[109] Merrouche A, Talbert T, Matt D, Martiré T, Pellecuer G. Interconnection of renewable sources: Multi-active-bridge converter. In: 2024 IEEE international conference on industrial technology. IEEE; 2024, p. 1–5.

[110] Khosroshahi A, Abapour M, Sabahi M. Reliability evaluation of conventional and interleaved DC–DC boost converters. IEEE Trans Power Electron 2014;30(10):5821–8.

[111] Murken M, Gratzfeld P. Reliability comparison of bidirectional automotive DC/DC converters. In: 2017 IEEE 86th vehicular technology conference (VTC-fall). IEEE; 2017, p. 1–7.

[112] Song Y, Schirmer PA, Schreivogel P, Zhang K, Wang H, Blaabjerg F. On the sensitivity analysis in reliability evaluation for power electronic converters. IEEE Trans Power Electron 2025.

[113] Parache F. Méthodologie de suivi et caractérisation du vieillissement d'électrolyseurs soumis à des courants variables [Ph.D. thesis], Université de Toulouse; 2024.

[114] Miličić T, Puteanus S, Becker X, Bernet S, Vidaković-Koch T. Predicting electrolyzer performance under forced periodic operation using nonlinear frequency response method. Appl Energy 2025;396:126312.

[115] Xu H, Ma J, Xue F, Li X, Li H, Wang W, Zhong Y, Zhao J, Zhang Y. Optimization control strategy for photovoltaic/hydrogen system efficiency considering the startup process of alkaline electrolyzers. Int J Hydrog Energy 2025;106:65–79.

[116] Makhsoos A, Kandidayeni M, Boulon L, Pollet BG. A comparative analysis of single and modular proton exchange membrane water electrolyzers for green hydrogen production-a case study in Trois-Rivières. Energy 2023;282:128911.

[117] Qi X, Gong M, Zhang J, Yang H. Power allocation strategy of multi-stack PEM electrolyzer for photovoltaic-hydrogen system considering the degradation of components in the electrolyzer. Electr Power Syst Res 2026;254:112653.

[118] Meynard TA, Renaudineau H, Canales PS, Kouro S, Concha D, Llor AM, Fadel M, Schneider H. TransformerLess partial voltage DC-DC converter with double power processing capacity. IEEE Open J Ind Electron Soc 2025.

[119] Guilbert D, Vitale G. Improved hydrogen-production-based power management control of a wind turbine conversion system coupled with multistack proton exchange membrane electrolyzers. Energies 2020;13(5):1239.

[120] Lu X, Du B, Zhou S, Zhu W, Li Y, Yang Y, Xie C, Zhao B, Zhang L, Song J, et al. Optimization of power allocation for wind-hydrogen system multi-stack PEM water electrolyzer considering degradation conditions. Int J Hydrog Energy 2023;48(15):5850–72.

[121] Pizarro P, Espina E, Diaz M, Ravet T, Rojas A, Carrasco D. A new modular multilevel converter topology for green hydrogen production. In: 2023 IEEE CHILEAN conference on electrical, electronics engineering, information and communication technologies. IEEE; 2023, p. 1–6.

[122] Rausell E, Navarro G, Lafoz M, Arnaltes S, Rodríguez JL, Blanco M, Nájera J. Analysis of using MMC topologies for the direct integration of renewable generation with modular electrolyzers. In: 2023 25th European conference on power electronics and applications (ePE'23 ECCE europe). IEEE; 2023, p. 1–8.